

**Asymptotic scaling properties and estimation of the generalized Hurst exponents in financial data**R. J. Buonocore,<sup>1,\*</sup> T. Aste,<sup>2,3</sup> and T. Di Matteo<sup>1,2</sup><sup>1</sup>*Department of Mathematics, King's College London, The Strand, London, WC2R 2LS, United Kingdom*<sup>2</sup>*Department of Computer Science, University College London, Gower Street, London, WC1E 6BT, United Kingdom*<sup>3</sup>*Systemic Risk Centre, London School of Economics and Political Sciences, London, WC2A2AE, United Kingdom*

(Received 27 April 2016; published 14 April 2017)

We propose a method to measure the Hurst exponents of financial time series. The scaling of the absolute moments against the aggregation horizon of real financial processes and of both uniscaling and multiscaling synthetic processes converges asymptotically towards linearity in log-log scale. In light of this we found appropriate a modification of the usual scaling equation via the introduction of a filter function. We devised a measurement procedure which takes into account the presence of the filter function without the need of directly estimating it. We verified that the method is unbiased within the errors by applying it to synthetic time series with known scaling properties. Finally we show an application to empirical financial time series where we fit the measured scaling exponents via a second or a fourth degree polynomial, which, because of theoretical constraints, have respectively only one and two degrees of freedom. We found that on our data set there is not clear preference between the second or fourth degree polynomial. Moreover the study of the filter functions of each time series shows common patterns of convergence depending on the momentum degree.

DOI: [10.1103/PhysRevE.95.042311](https://doi.org/10.1103/PhysRevE.95.042311)**I. INTRODUCTION**

The multifractal behavior of the financial time series is one of the acknowledged stylized facts in the literature (see Refs. [1–5]). Many works have been dedicated to its empirical characterization [6–23], reporting strong evidence of its presence in financial markets. Several models have been proposed [24–33] to reproduce these empirical facts.

Multifractality proved to be a very valuable tool. From a theoretical point of view models with a multifractal nature display also power law tails and volatility clustering, leading to consider these well-known stylized facts as consequences of the multifractal nature of financial time series. From a practical point of view multifractal models proved also to have forecasting power [26,34–36].

Many estimation methods are present in the literature; in particular the most popular are Multifractal Detrended Fluctuation Analysis (MFDFA) [37], the Generalized Hurst Exponent Method (GHE) [4,38–40], and Wavelet Transform Modulus Maxima (WWTM) [41]. All of them have advantages and drawbacks: MFDFA, which measures the scaling of the so-called fluctuation function, is applicable to nonstationary time series but the degree of the detrending method is arbitrary; GHE computes directly the scaling of the moments with respect to the aggregation horizon but the measurements are aggregation horizon dependent; and WWTM has a deep mathematical formulation which makes a parallelism with the thermodynamic and computes the scaling of a partition function defined in terms of WTMM coefficients but the choice of the wavelet function is arbitrary again. Moreover all these methods deal with the study of the scaling of a certain quantity against another one, but none of them gives a prescription on how to properly choose the scaling region and why certain regions should be discarded.

The aim of this paper is to propose a method for the estimation of the scaling behavior of the moments of real financial time series with respect to the aggregation horizon, without the need of free parameters, and which gives a precise prescription of the scaling region which has to be considered. In a previous paper [42], solving an ongoing debate in the literature (see, for example, Refs. [43–45]), it has been clarified that the true source of the multifractal behavior found in empirical financial time series is their causal structure. However, it was also shown that the measure of multifractality performed via the scaling of the moments in log-log scale is aggregation horizon dependent and that the true multifractal scaling should be measured in the limit of an infinite aggregation horizon. In particular, already for processes with i.i.d. increments but with power law tails in their distribution with exponents between two and five, which is the range empirically observed [46], due to the slow convergence of the Central Limit Theorem, the small aggregation horizon is affected by strong biases [42]. In light of this, we now face the problem of building up an estimation procedure able to address these issues and to reduce as much as possible these biases by proposing a reliable proxy of the asymptotic multifractal behavior of real financial time series. For reasons that are detailed later in the paper the method is well suited for intraday high-frequency data; in particular in this paper we focus on tick-by-tick data.

The structure of the paper is as follows: in Sec. II we recall the geometrical and statistical definitions of multifractality, in Sec. III we discuss the main features of the models we use in the paper to validate the proposed method, in Sec. IV we discuss the effect of the discreteness of processes on scaling measures, in Sec. V we introduce the method, in Sec. VI we show a step-by-step application of the method on a synthetic process with known multifractal properties, in Sec. VII we perform first a step-by-step application of the method to one real financial time series and then we apply it to different real time series, and in Sec. VIII we draw conclusions.

\*riccardo\_junior.buonocore@kcl.ac.uk

## II. MULTIFRACTALITY

In this section we give an overview on what is multifractality from a mathematical point of view and give its geometrical and statistical characterization.

### A. Geometrical characterization

Let  $X(t)$  be a process continuous in time with stationary increments. The notion of local Hölder exponent  $h(t)$  can be introduced via the following expression [47]:

$$|X(t + dt) - X(t)| \sim C(t)(dt)^{h(t)}, \quad (1)$$

where  $C(t)$  is a function of  $t$  and  $dt$  is an infinitesimal quantity which tends to zero. Also, in order to ensure that stationarity holds almost surely, the set on which  $C(t)$  and  $h(t)$  vary has zero Lebesgue measure. Intuitively the local Hölder exponent quantifies the local degree of singularity of a time series [47]. The set of all local Hölder exponents thus expresses the degree of singularity of the whole process  $X(t)$  associating a number at every point in time. In order to characterize the distribution of the local Hölder exponents, the notion of a singularity spectrum  $D(h)$  was introduced (cf. Refs. [47–49]). It is defined, for a given value  $\bar{h}$ , as

$$D(\bar{h}) = D_H\{t : h(t) = \bar{h}\}, \quad (2)$$

where  $D_H$  means the Hausdorff (or fractal) dimension of the set in curly brackets. So the singularity spectrum codifies the fractal dimension of the points sharing the same degree of singularity (Hölder exponent) [47–49].<sup>1</sup> If only one Hölder exponent, say,  $h_0$ , characterizes the process, then the process is said to be mono- or unifractal, and the singularity spectrum reads as [50]

$$D(h) = \begin{cases} 1 & h = h_0 \\ -\infty & \text{otherwise,} \end{cases} \quad (3)$$

so the spectrum reduces to a single point. A process is said to be multifractal if it has a range of values of  $h$  over which  $D(h) \geq 0$  [47,50].

### B. Statistical characterization

It turned out that the geometrical properties of a process can be linked to its statistical ones. In particular so-called Multifractal Formalism was introduced [48,49] and can be applied in the context of the stochastic processes [47]. Taking again the stationary, continuous in time, process  $X(t)$  and computing its increments over a time horizon  $\tau$ , it can be shown that, if the following scaling relation holds [51]:

$$E[|X(t + \tau) - X(t)|^q] = K(q)\tau^{\zeta(q)}, \quad (4)$$

where both  $K(q)$  and  $\zeta(q)$  are functions of  $q$  and  $\zeta(q)$  is concave [24], then  $D(h)$  and  $\zeta(q)$  are simply linked via a Legendre transform (see, for example, Refs. [5,47]),

$$\zeta(q) = 1 + \inf_h \{qh - D(h)\}, \quad (5)$$

$$D(h) = 1 + \inf_q \{hq - \zeta(q)\}. \quad (6)$$

The request of concavity is crucial for this result since otherwise the Legendre transform would not be well defined.

In practical situation one does not deal with processes in time. As a consequence, it was shown [5,48] that the straightforward estimation of  $D(h)$  cannot be practically achieved. In light of this, the importance of relations (5) and (6) relies on the fact that they allow us to estimate a geometrical quantity (the singularity spectrum) via statistical measurements. In particular one assumes that a real process (for example a log-price) is a discretized version of an underlying unobservable process continuous in time, which are sharing the same statistical properties. Thus, while geometrical arguments cannot be applied to the discrete version, statistical ones are. Usually the function  $\zeta(q)$  is rewritten as  $\zeta(q) = qH(q)$ , with  $H(q)$  called the Generalized Hurst Exponent [4,38,39]. In particular, from Eq. (6) (in order to find the minimum) we obtain the following chain of equalities:

$$h = \frac{d\zeta(q)}{dq} = H(q) + q \frac{dH(q)}{dq}, \quad (7)$$

which shows that the Hölder exponent is equal to the Hurst exponent only when the latter does not depend on  $q$ , which is the case of unifractal time series where  $\zeta(q)$  reduces to a straight line. The two most notable unifractal processes are Brownian motion (BM) and fractional Brownian motion (fBM), which satisfy respectively  $\zeta(q) = q/2$ , thus  $H(q) = 0.5$ , and  $\zeta(q) = qH$ , thus  $H(q) = H$  (see, for example, Ref. [4]).

## III. MODELS

In this section we summarize the main properties of the synthetic processes we use throughout the paper in order to validate the method we introduce in Sec. V.

### A. Brownian motion with Student's $t$ innovations (tBM)

We here introduce a uniscaling process with i.i.d. increments drawn from a Student's  $t$  distribution. Using the dummy variable  $t$ , we can write the probability density of a Student's  $t$  distribution as (see, for example, Ref. [52])

$$p(t) = \frac{\Gamma(\frac{n+1}{2})}{\sqrt{n\pi}\Gamma(\frac{n}{2})} \left(1 + \frac{t^2}{n}\right)^{-\frac{(n+1)}{2}}, \quad (8)$$

where  $\Gamma(\cdot)$  is the gamma function and  $n$  is the number of degrees freedom which are allowed to be noninteger. According to Eq. (8) if  $n > 1$ , the variable  $t$  has mean zero, otherwise it is infinite. The variance instead equals  $\frac{n}{n-2}$  if  $n > 2$  and infinite if  $1 < n < 2$ , and it is undefined otherwise. As for the spectrum of a tBM, it can be computed analytically in both cases, if either  $n$  is bigger or smaller than two. When  $n < 2$  the Student's  $t$  distribution of Eq. (8) becomes a stable distribution with skewness parameter equal to zero and stability parameter equal to  $n$ . So its scaling exponents can be readily written as

<sup>1</sup>We report that in Refs. [47,50] other two definitions can be found.

(see Refs. [37,53,54])<sup>2</sup>

$$\zeta(q) = qH(q) = \frac{q}{n} \quad \text{if } q < n. \quad (9)$$

For  $n > 2$  and finite aggregation horizon  $\tau$  it can be shown, as a corollary of the Central Limit Theorem (CLT), that

$$E[|X(t + \tau) - X(t)|^q] = f(q)\tau^{\frac{q}{2}}, \quad (10)$$

where  $f(q)$  is a function of  $q$ . Thus

$$\zeta(q) = qH(q) = \frac{q}{2}. \quad (11)$$

For  $n > 2$  the absolute moments of a tBM scale as those of a BM. For  $n = 2$ , it can be proved rigorously that the scaling exponents behave like Eq. (11) (cf. Ref. [55]).

Summarizing, a tBM is a unifractal process for both  $n < 2$  and  $n \geq 2$  with  $\zeta(q)$  behaving as a straight line with slopes respectively  $1/n$  and  $1/2$ .

### B. Multifractal random walk (MRW)

Different multifractal models have been proposed in the literature; however, in the present paper we chose as our benchmark multifractal model the so-called Multifractal Random Walk introduced in Ref. [30] since it has exactly computable scaling exponents. Despite further development and alternative multifractal random walks models with different scaling exponents that have been proposed (see Refs. [32,33]), for our purposes the statistical properties of this original model are sufficient. The process  $X(t)$  described by the model is defined as the limit  $\Delta t \rightarrow 0$  of the discretization step  $\Delta t$  of (see Ref. [30])

$$X(t) = \sum_{k=1}^{\frac{t}{\Delta t}} \epsilon_{\Delta t}(k) e^{\omega_{\Delta t}(k)}, \quad (12)$$

with  $\epsilon_{\Delta t} \sim N(0, \sigma^2 \Delta t)$ ,  $\omega_{\Delta t} \sim N(-\lambda^2 \ln(L/\Delta t), \lambda^2 \ln(L/\Delta t))$ , where  $\lambda$  is called intermittency parameter,  $L$  is the autocorrelation length, and  $\sigma$  is the variance of the overall process [30]. The increments of this process can then be written as

$$r_{\tau}(t) = X(t + \tau) - X(t) = \sum_{k=\frac{t}{\Delta t}+1}^{\frac{t+\tau}{\Delta t}} \epsilon_{\Delta t}(k) e^{\omega_{\Delta t}(k)}. \quad (13)$$

What characterizes this model is the autocorrelation structure, in particular the  $\epsilon_{\Delta t}(k)$  are i.i.d and the  $\omega_{\Delta t}(k)$  are not, having autocovariance (see Ref. [30]):

$$\text{Cov}(\omega_{\Delta t}(k_1), \omega_{\Delta t}(k_2)) = \lambda^2 \ln \rho_{\Delta t}(k_1 - k_2), \quad (14)$$

with

$$\rho_{\Delta t}(k_1 - k_2) = \begin{cases} \frac{L}{(|k_1 - k_2| + 1)\Delta t} & |k_1 - k_2| < L/\Delta t, \\ 1 & \text{otherwise.} \end{cases} \quad (15)$$

<sup>2</sup>In Ref. [37] the shape of the scaling exponent for  $q > n$  is reported to be equal to one. However, as underlined in Refs. [53] and [54], this so-called bifractal behavior is a pure finite size sample effect.

The scaling exponents of this model in the continuous time limit are (see Ref. [30])

$$\zeta(q) = qH(q) = -\frac{\lambda^2}{2} q^2 + \left(\lambda^2 + \frac{1}{2}\right) q. \quad (16)$$

What makes this model very appealing for statistical testing is that it exhibits both power law tails and volatility clustering, keeping its plain innovations uncorrelated despite having only three parameters ( $\lambda, L, \sigma$ ) in its definition. In particular the intermittency parameter  $\lambda$  determines both the power law tails, which decay with an exponent proportional to  $\lambda^2$  (see Ref. [56]), and the decay of the autocorrelation functions of the powers of the absolute returns, whose decaying exponents are again proportional to  $\lambda^2$  (see Ref. [30]).

## IV. THE CURSE OF THE DISCRETIZATION

As underlined in Sec. II B the introduction of the multifractal formalism allows us to study the geometrical fractal properties of a process by analyzing its discrete version. However, as shown in Ref. [42], the estimation of the scaling exponents turned out to be strongly biased. Convergence issues arise for both power law-tailed and autocorrelated discrete processes, for both synthetic and real data. In this section we discuss in more detail these two features in the case of synthetic processes, which in turn will justify our choice of introducing the filter function in Sec. V. The need of the filter function also for real financial process will become evident in Sec. VII where we apply our method to real data.

### A. Effect of the CLT

In Ref. [42] it was pointed out that for processes with independent increments, power law tails, and finite variance, the asymptotic convergence is obviously ruled by the CLT. We want to show results showing the actual numerical behavior of this convergence. Let us then consider a discrete process with independent increments  $x_i$  i.i.d. distributed according to a certain pdf  $p(x_i)$  for all  $i$  such that

$$E[x_i] = 0, \quad \text{Var}[x_i] = \sigma^2 \Delta t < \infty, \quad (17)$$

for some constant  $\sigma$ , where  $\Delta t$  is the time interval between two increments. Let us stress that we are not making any assumption on  $p(x_i)$  which can be skewed, power law-tailed, or both as long as the variance is finite. For example, it could be the density of a shuffled empirical time series. We now introduce the quantity

$$S_N = \sum_{i=1}^N x_i, \quad (18)$$

which is an the aggregated sum of  $N$  returns, thus

$$E[S_N] = 0, \quad \text{Var}[S_N] = \sum_{i=1}^N \text{Var}[x_i] = \sigma^2 N \Delta t, \quad (19)$$

so the variance grows linearly with time as expected. We stress now that the quantity we use to measure the scaling of empirical time series is exactly  $E[|S_N|^q]$ . In this case we are considering it for a shuffled or independent process. The scaling properties of  $S_N$  are a straightforward consequence

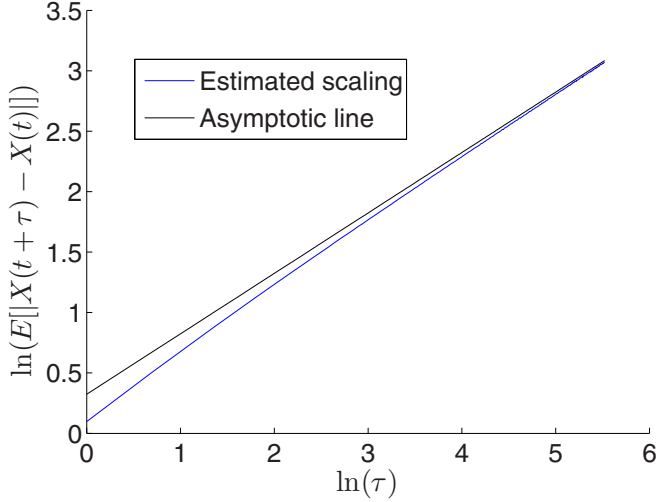


FIG. 1. Blue solid line: numerical scaling of  $E[|S_N|]$  for a tBM with  $n = 3$  [cf. Eq. (A3)] with  $q = 1$ ; black solid line: theoretical expectation in the continuous limit.

of the CLT. It can be shown (see Appendix A for an explicit computation) that

$$E[|S_\infty|^q] = \lim_{\substack{\Delta t \rightarrow 0 \\ N \rightarrow \infty \\ N\Delta t = \tau}} E[|S_N|^q] = \sigma^q \frac{2^{\frac{q}{2}} \Gamma(\frac{q+1}{2})}{\sqrt{\pi}} \tau^{\frac{q}{2}}. \quad (20)$$

Equation (20) proves rigorously that any i.i.d. process with finite variance aggregates asymptotically into a unifractal process, and in particular it scales as a BM (we underline that it holds also for shuffled empirical financial time series). As a corollary, this also shows that empirical multifractality can arise only from a nontrivial causal structure.

### 1. First example: Power law tails

We apply here Eq. (20) to the case of tBM. For our purposes we chose the number of degrees of freedom to be equal to  $n = 3$ , and, in order to remove as much noise as possible, we generated a time series made of  $10^7$  steps. For a tBM, Eq. (20) tells everything about its asymptotic behavior. In particular, with  $n = 3$  and  $q = 1$ ,

$$E[|S_\infty|] = \sqrt{\frac{6}{\pi}} \tau^{\frac{1}{2}}, \quad (21)$$

thus

$$\ln(E[|S_\infty|]) = \frac{1}{2} \ln(\tau) + \ln\left(\sqrt{\frac{6}{\pi}}\right). \quad (22)$$

In Fig. 1 we superpose the theoretical behavior of Eq. (22) with the numerical one.

As appears evident, the linearity is achieved only asymptotically [cf. the effect of the productory in Eq. (A3)].

### 2. Second example: Shuffled MRW

In this subsection we apply Eq. (20) in the case of shuffled MRW. We set the parameters to  $\lambda = 0.3$ ,  $L = 5000$ , and  $\sigma = 1$

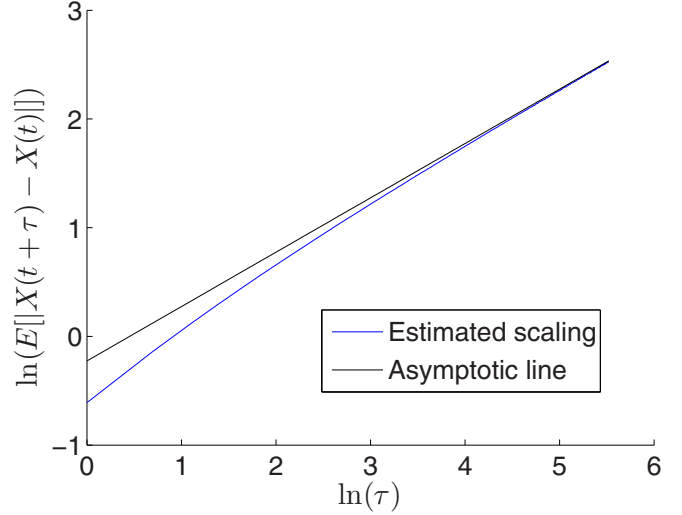


FIG. 2. Blue solid line: numerical scaling of  $E[|S_N|]$  for a shuffled MRW [cf. Eq. (A3)] with  $q = 1$ ; black solid line: theoretical expectation in the continuous limit.

(because of the shuffling the choice of the values of  $\lambda$  and  $L$  may be arbitrary while  $\sigma$  is simply a scale), and again we generated a time series made of  $10^7$  steps to remove as much noise as possible. In Fig. 2 we superpose the theoretical behavior of Eq. (20) with the numerical one for  $q = 1$ .

As appears evident, the linearity is achieved again only asymptotically [cf. the effect of the productory in Eq. (A3)].

## B. Effect of the autocorrelation

In Ref. [42] it is proven numerically that the autocorrelation is the true source of the empirical multifractality. In the same direction is the result of Sec. IV A, which proves that the shape of the distribution plays no role in the asymptotic scaling as long as the variance is finite. However, for small aggregation horizons scaling measures are strongly biased also when the effect of the tails is removed (see Ref. [42]). These observations lead to the puzzling conclusion that the causal structure is, from the theoretical point of view, the source of the multifractal nature of a process but, from a numerical point of view, also the source of a bias. In order to reconcile these results let us consider the case of the MRW. A first observation is that Eq. (16) holds in the continuous time limit, whereas synthetic and real processes are inherently discrete in time. A second observation is that the innovations of the discretized version of the MRW, shown in Eq. (13), are conditionally Gaussian, whereas the distribution of the innovations in the continuous time limit has power law tails (cr. Ref. [35]). It is worth noting that in this case a continuous time limit means aggregating an infinite number of conditionally Gaussian variables with a certain memory structure given by Eq. (14). Thus, for the MRW, the mismatch arises because the discrete process in Eq. (13) is not a multifractal process described by the scaling exponents in Eq. (16), but its infinite aggregation limit (continuous time limit) is.

We propose that the same feature also holds for real financial processes, by arguing that the distribution of the returns at their smallest considered scale (for example, tick-by-tick)

is different from their distribution at large aggregations. For instance, one evident difference between returns taken on a tick-by-tick basis and, say, daily returns is the role of the tick size [57]. In the first case the returns have discrete values, while in the second case they can be safely modeled as continuous.

As a corollary of these observations, we observe that for the BM and the fBM the convergence issues are not present because the distribution of the increments in the discrete version of the processes are Gaussian as the distribution of the increments in the continuous time limit; i.e., they are described by a distribution stable under aggregation.

## V. BUILDING A SCALING EXPONENTS PROXY

In this section we provide a procedure to estimate the scaling exponent of a given time series. It is made up of two parts: the first consists in giving a reliable parameter-free estimate of the set of scaling exponents taking into account the convergence issues discussed above, and, in the second, a fit of the measured scaling exponents is performed, allowing then to smooth them according to the theoretical prescriptions of the multifractal picture.

### A. Taking into account the convergence issues

As shown in the previous section, the scaling properties of a time series are completely uncovered only in the limit of infinite aggregation. In practical situations this condition is obviously unrealistic. In particular, for a process continuous in time, the condition of infinite aggregation of the increments is already satisfied at any finite aggregation horizon, while for a discrete time series the infinite aggregation request translates into an infinite aggregation horizon. It thus seems that the multifractal properties of a discrete time series are theoretically uncovered only asymptotically. Let us consider then the logarithm of Eq. (4):

$$\ln\{E[|X(t+\tau) - X(t)|^q]\} = \zeta(q)\ln(\tau) + \ln[K(q)]. \quad (23)$$

In Ref. [42] it was proven that the scaling measures are horizon dependent; in other words the results change with  $\tau$ , reconciling with the theoretical expectations for large values of  $\tau$ . It means in particular that the scaling is not exactly linear. In light of this we argue that for discrete processes the right-hand side of Eq. (23) is an oblique asymptote. In other words, Eq. (23) holds exactly for every  $\tau$  only for processes continuous in time, while for discrete ones a correction is needed due to the convergence issues. Let us define then  $x = \ln(\tau)$  and  $f(x) = \ln\{E[|X(t+\tau) - X(t)|^q]\}$  for a given value of  $q$ . Using these variables the usual fit performed in order to unveil the scaling structure of a time series is

$$f(x) = mx + z, \quad (24)$$

where then  $m = \zeta(q)$  is the quantity we are interested in and  $z$  is the logarithm of the  $q$  moment for  $\tau = 1$ . We propose now instead to take into account the convergence issues by generalizing Eq. (24) as

$$f(x) = g(x) + mx + z, \quad (25)$$

where  $g(x)$  is a correction function which we call filter function, which models the convergence toward the asymptotic

behavior. Coherently with the previous section, Eq. (25) has to satisfy the condition  $g(x) \xrightarrow{x \rightarrow \infty} 0$ . For real time series, determining the actual shape of  $g(x)$  is a hard task; however, we developed a data-driven method which allows us to take into account the presence of  $g(x)$  without computing it explicitly.

### B. Taking advantage of the convergence issues

The first step is considering the integral of the signal. This implies that the scaling is now supposed to be given by the integral of Eq. (25),

$$\begin{aligned} F(x) &= \int_0^x [g(x') + mx' + z] dx' \\ &= \int_0^x g(x') dx' + \frac{m}{2} x^2 + zx, \end{aligned} \quad (26)$$

which is a parabola plus the integral of the filter function. Let us now assume that the filter function has a finite integral over the positive real axis,<sup>3</sup>

$$\int_0^\infty g(x) dx = \text{const}, \quad (27)$$

which we will prove numerically below during applications. So it follows that

$$F(x) \xrightarrow{x \rightarrow \infty} \frac{m}{2} x^2 + zx + \text{const}. \quad (28)$$

We fit then the integrated empirical scaling with a parabolic shape:

$$p(x) = ax^2 + bx + c. \quad (29)$$

Theoretically it should be in perfect agreement with the empirical scaling in the interval<sup>4</sup>  $[\tau^*, \infty)$  with  $\tau^* \gg 1$ . Varying then  $\tau^*$  between 1 and  $\infty$ , we expect the term of degree zero in Eq. (29), i.e.,  $c(\tau^*)$ , to reach asymptotically a plateau since it represents the area between the empirical scaling and the asymptotic linear scaling. Three scenarios are possible: if the empirical scaling tends to the asymptote from above, we expect  $c(\tau^*)$  to be positive since the integral of the filter function is a positive number; if the empirical scaling tends to the asymptote from below, we expect  $c(\tau^*)$  to be negative since the integral of the filter function is a negative number; and if the empirical scaling oscillates around the asymptote before converging on it, we expect  $c(\tau^*)$  to present maxima and minima.

### C. Finding the maximum value of the aggregation

However, due to the finiteness of empirical samples a maximum value of aggregation,  $\tau_{\max}$ , has to be found. Moreover, from a theoretical point of view the multifractal scaling holds only as long as the causal structure plays a role (cf. Ref. [42]). In light of this we infer that a good proxy for the value of  $\tau_{\max}$  is the autocorrelation length. It is known (cf. Ref. [58,59]) that, given an iid discrete process of length  $T$ , say,  $|r_\tau(t)|^q$ , its autocorrelation function behaves asymptotically as

<sup>3</sup>We recall that  $g(x) \xrightarrow{x \rightarrow \infty} 0$  by definition, which is a necessary but not sufficient condition for the convergence of its integral.

<sup>4</sup>We recall that  $x = \ln(\tau)$ .

a normally distributed noise,  $N(0, 1/T)$ . In light of this, the most common choices for cutting its autocorrelation profile are the following:

- (1) The first lag when the autocorrelation function of  $|r_\tau(t)|^q$  reaches the 99th percentile of the noise distribution
- (2) The first lag when the autocorrelation function of  $|r_\tau(t)|^q$  reaches the 99th percentile of the noise distribution
- (3) The first lag when the autocorrelation function of  $|r_\tau(t)|^q$  reaches the 50% percentile (zero level) of the noise distribution.

Since fixing one of these criteria would be arbitrary, for empirical data we apply all three prescriptions running our algorithm for all of them, deciding afterwards the best of the three using a criterion we discuss in a following subsection based on the root-mean-square error. We report, however, that in general, given a certain value of  $\tau_{\max}$ , it is always a good habit to check the empirical scaling in loglog scale and, if linearity does not hold, reduce  $\tau_{\max}$  accordingly.

**D. Finding the minimum value of the aggregation**

Let us now describe how the value of  $\tau_{\min}$  is fixed. Going back to the function  $c(\tau^*)$ , fixing a maximum value means that now finite size effects occur. In particular we found that when  $\tau^*$  approaches  $\tau_{\max}$ ,  $c(\tau^*)$  starts to wildly oscillate because the number of points over which the fit is performed becomes too small. Thus we need to understand which value of  $c(\tau^*)$  gives us a good approximation of its asymptotic behavior, which in turn would give us information about  $\tau_{\min}$ . In principle we do not know if the empirical scaling will settle on its asymptote from above or below (maybe oscillating before); however, we expect a good approximation of its asymptotic behavior to be given either by one of its maxima, if it finally settles from above, or by one of its minima, if it finally settles from below. In order to make a statistically meaningful decision, we prescribe to take, among the set of all maxima and minima of  $c(\tau^*)$ , the one which attains the maximum value of the adjusted coefficient of determination [60]. We call the value of  $\tau^*$  where

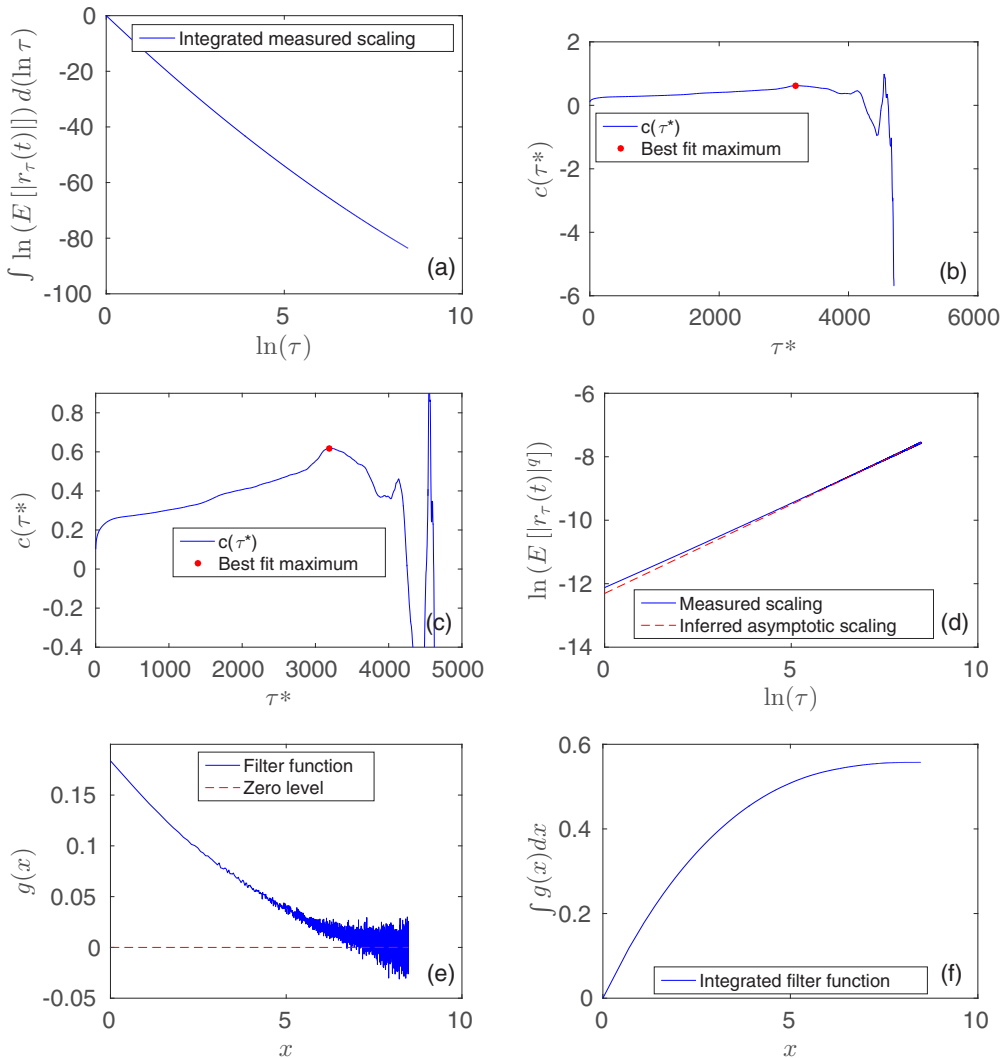


FIG. 3. (a) Integrated measured scaling [cf. Eq. (26)]; (b) in blue solid line  $c(\tau^*)$  and the maximum where the best parabolic fit is attained marked with a red or shaded dot [cf. Eqs. (28) and (29)]; (c) zoom of the behavior of  $c(\tau^*)$  around the maximum where the best parabolic fit is attained (red or shaded dot) [cf. Eqs. (28) and (29)]; (d) plain scaling in blue solid line and the asymptotic inferred scaling in red dashed line [cf. Eqs. (23) and (25)]; (e) filter function  $g(x)$  in blue solid line and the zero level in red dashed line; (f) integrated filter function [cf. Eq. (27)].

this maximum or minimum occurs  $\tau_{\min}$ . In order to avoid the method to detect spurious maxima or minima) due to noise in the scaling we add the condition that the  $\tau_{\min}$  have to be such that  $H(q) = 2a(\tau_{\min})/q > 0.5$  to ensure the concavity of the function  $\zeta(q)$ . Once both the values of  $\tau_{\min}$  and  $\tau_{\max}$  are fixed, the best linear fit of the scaling of the considered moment can be performed in the range  $[\tau_{\min}, \tau_{\max}]$ , where the slope gives the value of scaling exponent itself.

### E. Fitting the scaling exponents

The procedure described up to now is completely parameter-free and allows us to estimate single scaling exponents. In order to smooth the measured scaling exponents coherently with the multifractal picture requirement and to make a quantitative assessment about the overall shape of the empirical functions  $\zeta(q)$ , we decided to perform a polynomial robust fit, using the least absolute residuals method (see Ref. [61]), with  $q$  between  $-0.9$  and  $1$  every  $0.1$  units, extending then the prescription given in Ref. [42]. In particular we used a second and a fourth degree polynomials.<sup>5</sup> Let us first consider the latter:

$$\zeta(q) = Dq^4 + Cq^3 + Bq^2 + Aq + \text{const.} \quad (30)$$

In its most general form Eq. (30) has five degrees of freedom, however, the function  $\zeta(q)$  must satisfy few conditions, in particular

$$\begin{aligned} \zeta(0) &= 0 \\ \zeta(2) &= 1 \\ \zeta''(q) &< 0. \end{aligned} \quad (31)$$

The first condition follows directly from the definition of the scaling exponents (see Sec. II B); the second one, which implies  $H(2) = 0.5$ , follows from the absence of autocorrelation in the empirical financial returns (we give a simple proof of this in Appendix B); and the third one follows from the concavity condition (cf. Sec. II B and references). Applying these conditions to Eq. (30), they become respectively (we report the explicit computation of the third condition in Appendix C)

$$\begin{aligned} \text{const} &= 0 \\ A &= \frac{1}{2} - 8D - 4C - 2B \\ B &= \frac{3C^2}{8D} \text{ with } D < 0, \end{aligned} \quad (32)$$

so Eq. (30) can be rewritten as

$$\zeta(q) = Dq^4 + Cq^3 + \frac{3C^2}{8D}q^2 + \left(\frac{1}{2} - 8D - 4C - \frac{3C^2}{4D}\right)q \quad (33)$$

$D < 0,$

which has only two degrees of freedom,  $C$  and  $D$ . As for the second degree polynomial fit, in its most general form it reads as

$$\zeta(q) = Bq^2 + Aq + \text{const.}, \quad (34)$$

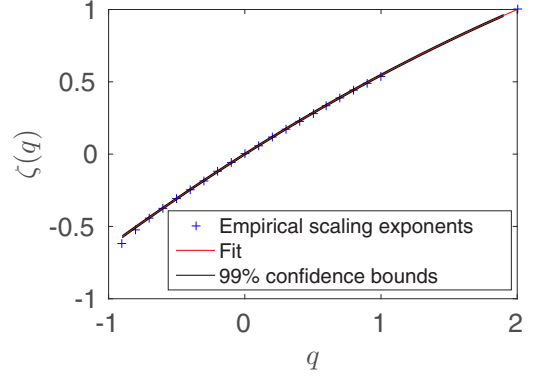


FIG. 4. Fitted measured scaling exponents for a realization of a MRW. Blue crosses: measured scaling exponents; red solid line: polynomial fit; black solid lines: 99% confidence intervals of the values of the fitted curve.

which then, enforcing conditions in Eq. (31), becomes

$$\begin{aligned} \zeta(q) &= Bq^2 + \left(\frac{1}{2} - 2B\right)q \\ B &< 0, \end{aligned} \quad (35)$$

having then only one degree of freedom. For each empirical time series we chose between the two fits checking the maximum value of the adjusted coefficient of determination (see Ref. [60]). At this point we have then a shape for each of the three proposed autocorrelation lengths given in Sec. V C. As a criterion to choose among them, we keep the fit which attains the least value of the root-mean-square error, in other words the one which leads to the least dispersion of the data around the fitted curve.

### F. Summary of the method

- (1) Given one prescription for the autocorrelation length (see Sec. V C), compute the value of  $\tau_{\max}$  for every measured  $q$  fixing then its value to be the maximum among them
- (2) Integrate the empirical scaling of the chosen  $q$ th absolute moments computed in  $\tau \in [1, \tau_{\max}]$

TABLE I. Results of the application of the method in order to compute  $H(-0.5)$ ,  $H(-0.3)$ ,  $H(-0.1)$ ,  $H(0.1)$ ,  $H(0.5)$ , and  $H(1)$  of a MRW with parameters  $\lambda = 0.3, 0.4, 0.5$   $L = 5000$ ,  $\sigma = 10^{-5}$ .

MRW	$\lambda = 0.3$	$\lambda = 0.4$	$\lambda = 0.5$
$\hat{H}(-0.5)$	$0.612 \pm 0.028$ (0.6125)	$0.696 \pm 0.033$ (0.7)	$0.795 \pm 0.042$ (0.8125)
$\hat{H}(-0.3)$	$0.607 \pm 0.035$ (0.6035)	$0.680 \pm 0.043$ (0.684)	$0.770 \pm 0.047$ (0.7875)
$\hat{H}(-0.1)$	$0.597 \pm 0.033$ (0.5945)	$0.665 \pm 0.038$ (0.668)	$0.748 \pm 0.042$ (0.7625)
$\hat{H}(0.1)$	$0.589 \pm 0.031$ (0.5855)	$0.648 \pm 0.033$ (0.652)	$0.725 \pm 0.037$ (0.7375)
$\hat{H}(0.5)$	$0.569 \pm 0.026$ (0.5675)	$0.617 \pm 0.023$ (0.62)	$0.679 \pm 0.029$ (0.6875)
$\hat{H}(1)$	$0.545 \pm 0.023$ (0.545)	$0.577 \pm 0.022$ (0.58)	$0.618 \pm 0.024$ (0.625)

<sup>5</sup>The third degree is ruled out by the concavity requirement.

(3) For each moment fix the value of  $\tau_{\min}$  observing the behavior of the term of degree zero of the parabolic fit [cf. Eq. (29) and Sec. VD]

(4) Infer the value of the scaling exponents via the best linear fit in the scaling regions [ $\tau_{\min}, \tau_{\max}$ ]

(5) Check that the filter function  $g(x)$  converges to zero and that its integral converges to a constant

(6) Perform a parabolic and a quartic fit, then decide the best among them checking the maximum adjusted coefficient of determination

(7) Repeat steps 1 to 6 for all three prescriptions for choosing  $\tau_{\max}$  (see Sec. VC) and select the one which gives the overall fit with the least root-mean-square error.

What is left is to prove that in the range [ $\tau_{\min}, \tau_{\max}$ ] chosen via this method, the filter function reaches a plateau, thus proving that its effect has been completely filtered out. This will be proved numerically below. In particular we will show

that this holds for the MRW, where the absolute moments scaling is computed for its increments [cf. Eq. (13)], and afterwards for empirical data, where the absolute moments scaling is computed for the log returns. We point out that for every  $\tau$  we remove the mean from every return time series since a nonzero mean would end up in the detection of spurious autocorrelations also due to possible nonstationarities. We report that this operation is justified by the financial assumption of zero returns on average.

### VI. APPLICATION TO SYNTHETIC DATA: VALIDATION OF THE METHOD

In this section we show the application of the method on a MRW, which has known multifractal properties, proving the capability of our method to capture, for example, the expected values of  $H(-0.5)$ ,  $H(-0.3)$ ,  $H(-0.1)$ ,  $H(0.1)$ ,  $H(0.5)$ , and

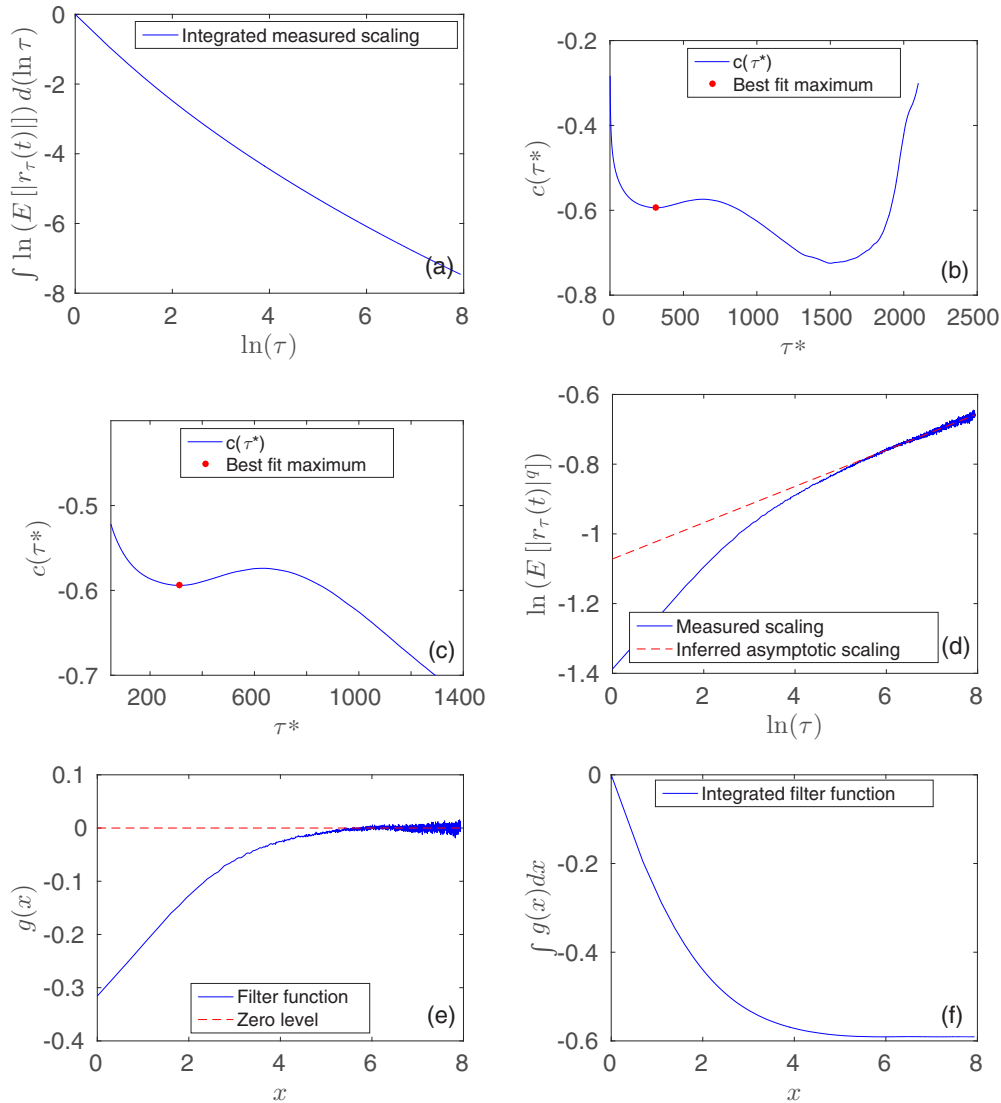


FIG. 5. Step-by-step application of the method for the scaling of  $H(0.1)$  for AXP. (a) Integrated measured scaling [cf. Eq. (26)]; (b) in blue solid line  $c(\tau^*)$  and the maximum where the best parabolic fit is attained marked with a red or shaded dot [cf. Eqs. (28) and (29)]; (c) zoom of the behavior of  $c(\tau^*)$  around the maximum where the best parabolic fit is attained (red or shaded dot) [cf. Eqs. (28) and (29)]; (d) plain scaling in blue solid line and the asymptotic inferred scaling in red dashed line [cf. Eqs. (23) and (25)]; (e) filter function  $g(x)$  in blue solid line and the zero level in red dashed line; (f) integrated filter function [cf. Eq. (27)].

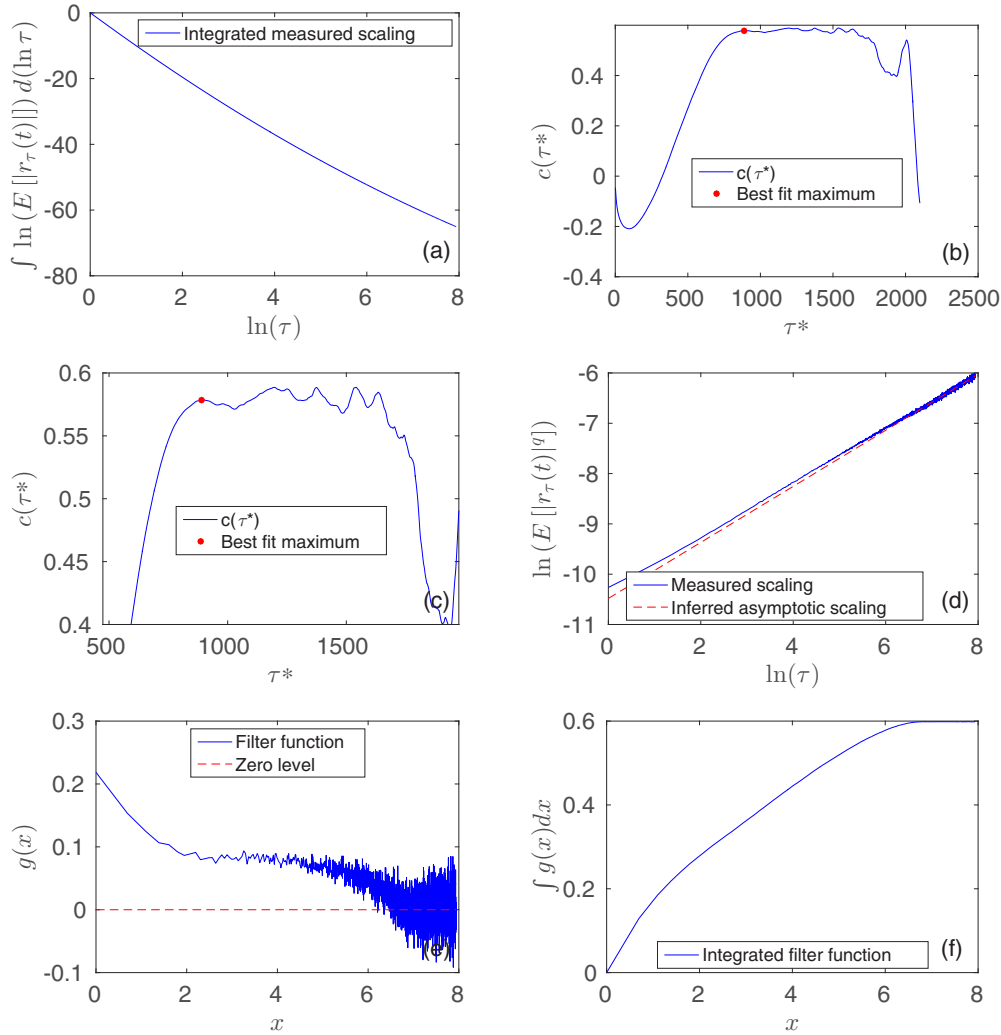


FIG. 6. Step-by-step application of the method for the scaling of  $H(1)$  for AXP. (a) Integrated measured scaling [cf. Eq. (26)]; (b) in blue solid line  $c(\tau^*)$  and the maximum where the best parabolic fit is attained marked with a red or shaded dot [cf. Eqs. (28) and (29)]; (c) zoom of the behavior of  $c(\tau^*)$  around the maximum where the best parabolic fit is attained (red or shaded dot) [cf. Eqs. (28) and (29)]; (d) plain scaling in blue solid line and the asymptotic inferred scaling in red dashed line [cf. Eqs. (23) and (25)]; (e) filter function  $g(x)$  in blue solid line and the zero level in red dashed line; (f) integrated filter function [cf. Eq. (27)].

$H(1)$ . As an example, in Fig. 3 are reported all the relevant steps of the application of the method for the computation of  $H(1)$  to a MRW made of  $N = 10^7$  steps,  $\lambda = 0.3$ ,  $L = 5000$ , and  $\sigma = 10^{-5}$ . The length of the time series was chosen to reduce as much as possible the noise, the value of  $\lambda$  to show clearly the convergence issues caused by the interplay between the power law tails and the volatility clustering, and  $L$  and  $\sigma$  to be comparable with their value measured on empirical tick-by-tick financial data. In particular we report, from left to right from top to bottom, the integrated measured scaling [cf. Eq. (26)], the whole shape of  $c(\tau^*)$  and the maximum where the best parabolic fit is attained [cf. Eqs. (28) and (29)], a zoom of the behavior of  $c(\tau^*)$  around the maximum where the best parabolic fit is attained [cf. Eqs. (28) and (29)], the plain scaling with the asymptotic inferred scaling [cf. Eqs. (23) and (25)], and the filter function  $g(x)$  and the integrated filter function [cf. Eq. (27)]. In order to choose the value of  $\tau_{\max}$  we fix it independently for each value of  $q$  using the cut of

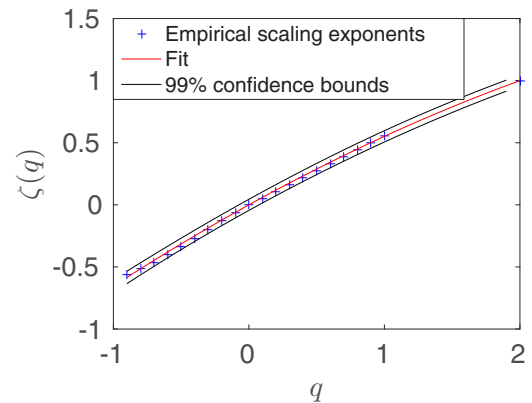


FIG. 7. Blue crosses: empirical scaling exponents; red solid line: polynomial fit; black solid lines: 99% confidence intervals of the values of the fitted curve.

TABLE II. Numerical results of the application of the method to empirical data. For each time series we report the ticker, the value of  $\hat{D}$  and  $\hat{C}$  or  $\hat{B}$ , and whether we found more appropriate a second or a fourth degree polynomial fit, along with the 95% confidence interval, the value of  $\tau_{\max}$ , and its length.

Ticker	$\hat{D}$	$\hat{C}$	$\hat{B}$	$\tau_{\max}$	No. of points
ABT			-0.0314 (-0.0330, -0.0298)	4761	733 160
ACN			-0.0185 (-0.0198, -0.0173)	2297	288 564
ADBE			-0.0125 (-0.0157, -0.0092)	3254	361 922
AIG	-0.0149 (-0.0274, -0.0024)	0.0049 (-0.02811, 0.038)		8323	979 380
AMD	-0.0353 (-0.0411, -0.0294)	0.1424 (0.1325, 0.1523)		1831	283 456
AXP			-0.0515 (-0.0578, -0.0452)	2798	626 710
GOOGL	-0.0524 (-0.0535, -0.0512)	0.1404 (0.1380, 0.1429)		1904	237 276
HON			-0.0254 (-0.0273, -0.0236)	4692	444 198
MAR	-0.0055(-0.0077, -0.0032)	-0.0185(-0.0192, -0.0177)		3504	317 754
MMM	-0.0091(-0.0121, -0.0061)	0.0065 (-0.0028, 0.0158)		2138	305 018
PG			-0.0622(-0.0642, -0.0601)	4661	946 435

the autocorrelation at the 99% confidence level. As appears evident from the figures,  $c(\tau^*)$  reaches a first maximum and then starts to oscillate. The left bottom figures prove that the filter function converges to zero for high values of  $x = \ln \tau$ , while the right bottom one that its integral actually converges, thus filling the gaps left opened in the previous section at least for this particular process. The numerically computed scaling (blue solid line in the middle right figure) appears to settle on the asymptotic inferred scaling from above (dashed red line). In Fig. 4 we report instead the whole spectrum.

In order to make a quantitative assessment we generated  $10^4$  MRWs made of  $10^6$  points and  $\lambda = 0.3, 0.4, 0.5, L = 5000, \sigma = 10^{-5}$  as before. On each of them we applied our method in order to compute  $H(-0.5), H(-0.3), H(-0.1), H(0.1), H(0.5),$  and  $H(1)$  and, since we found the estimators distributions are skewed, we report their median and median absolute deviation. We report the results in Table I along with the theoretical values between parenthesis in boldface under the measured values. The notation of the hat means the estimator of the quantity under it.

The measured values are in perfect agreement with the expected ones. In the next section we turn our attention to empirical data.

### VII. APPLICATION TO REAL FINANCIAL DATA

In this section we discuss the application to real financial data. In particular we make a few observations concerning the choice of the data set, we illustrate the method step by step on a specific data set while we show the final outcome of its application to various other data sets.

#### A. The choice of the data set

Nowadays trading takes place at high-frequency speed, which means that on a trading day on the order of hundreds of thousands transactions may occur. Moreover the number of transactions differs from day to day. As an example let us report the case of the trade log price of the American Express Company (AXP), taken tick-by-tick from 12 October 2015 to 11 November 2015 traded on working days between 9:30 and 16:30 at the New York Stock Exchange (NYSE) made of 626 710 points. The trading days in the given time span are 23, and we can check, for example, how many trades occurred in the day with the minimum amount of trades and how many trades occurred in the day with the maximum amount of

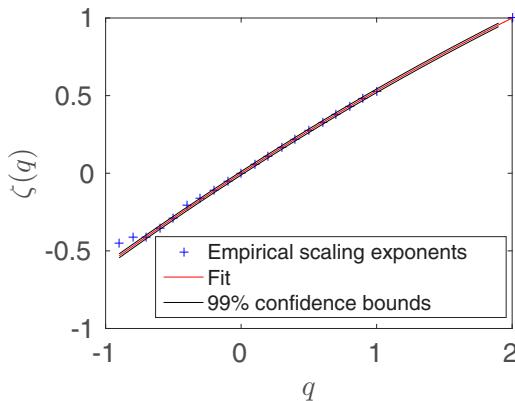


FIG. 8. Fitted empirical scaling exponents for ABT time series. Blue crosses: empirical scaling exponents; red solid line: polynomial fit; black solid lines: 99% confidence intervals of the values of the fitted curve.

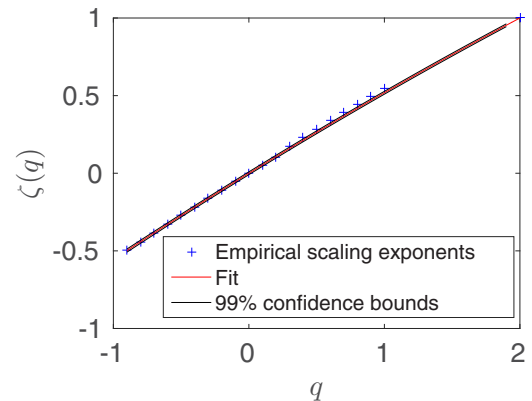


FIG. 9. Fitted empirical scaling exponents for ACN time series. Blue crosses: empirical scaling exponents; red solid line: polynomial fit; black solid lines: 99% confidence intervals of the values of the fitted curve.

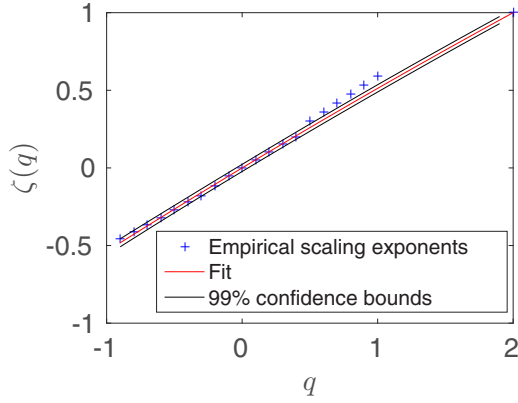


FIG. 10. Fitted empirical scaling exponents for ADBE time series. Blue crosses: empirical scaling exponents; red solid line: polynomial fit; black solid lines: 99% confidence intervals of the values of the fitted curve.

trades:

$$\begin{aligned} \text{minimum no. of trades} &= 10\,110 \\ \text{maximum no. of trades} &= 100\,133. \end{aligned} \quad (36)$$

In general we can say that, within a day, the second, minute, hourly, etc., returns are the result of the aggregation of the tick-by-tick returns (relative to the trading price). Thus if we consider the log price taken at a fixed time rate, for example every second, it becomes a subordinated process which inherits the statistical properties of its subordinator (the trading time) (cf. Ref. [62]), which we are in general not granting to be stationary. Moreover intraday data taken at a fixed time interval have strong seasonalities (cf. Ref. [2]), which are instead almost absent in their tick-by-tick version. Seasonalities actually can also be avoided analyzing daily data; however, the subordination feature mentioned above still holds, and a long time span is required to properly measure the multifractal scaling (cf. Ref. [42]). For example, in order to obtain a time series of roughly 25 000 steps, around 100 years are needed, which heavily clashes with the assumption

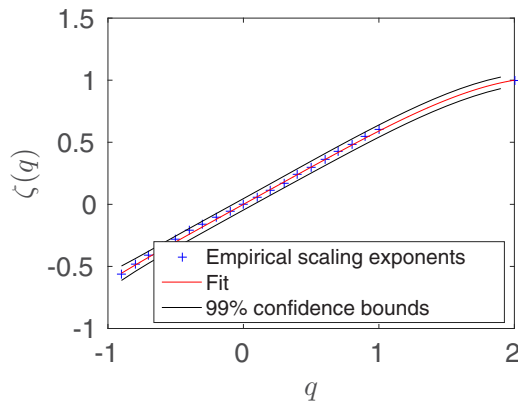


FIG. 11. Fitted empirical scaling exponents for AIG time series. Blue crosses: empirical scaling exponents; red solid line: polynomial fit; black solid lines: 99% confidence intervals of the values of the fitted curve.

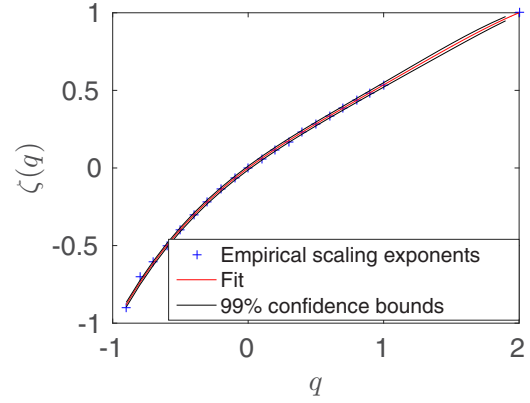


FIG. 12. Fitted empirical scaling exponents for AMD time series. Blue crosses: empirical scaling exponents; red solid line: polynomial fit; black solid lines: 99% confidence intervals of the values of the fitted curve.

of stationarity. We add also that, according to our analyses, in order to reach a level of aggregation informative of the asymptotic behavior, time series made of at least 200 000 steps are needed with an autocorrelation length of at least 1500 lags. Since these requirements are easily met by tick-by-tick data, we found quite a natural choice to limit our analysis to them. One last word has to be given to the fact that in the tick-by-tick regime data are intrinsically discrete since in markets there is a lower bound to the fraction of the currency we trade with. We notice, however, that our analysis focuses on the high aggregation regime where the returns are supposed to take continuous values.

### B. Numerical results: AXP

In this subsection we report the result of the application of our method for the computation of the scaling exponents of the AXP time series, focusing in particular on  $H(0.1)$  and  $H(1)$  as an example. Given the prescription in Sec. V C, the possible values of  $\tau_{\max}$  are

$$\tau_{\max}^{99\%} = 2798, \quad \tau_{\max}^{95\%} = 3507, \quad \tau_{\max}^{50\%} = 4201. \quad (37)$$

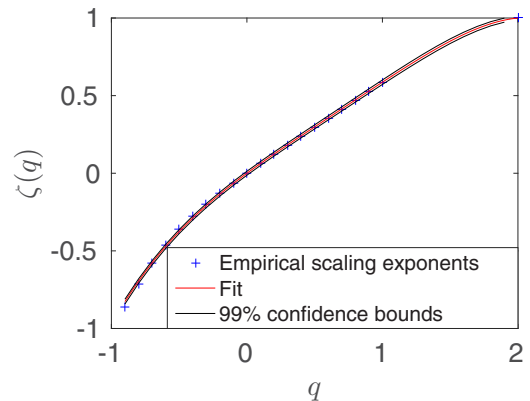


FIG. 13. Fitted empirical scaling exponents for GOOGL time series. Blue crosses: empirical scaling exponents; red solid line: polynomial fit; black solid lines: 99% confidence intervals of the values of the fitted curve.

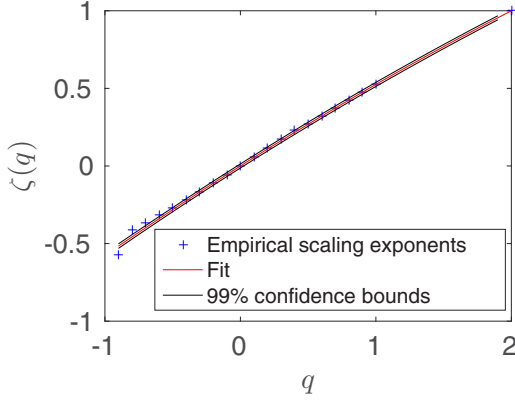


FIG. 14. Fitted empirical scaling exponents for HON time series. Blue crosses: empirical scaling exponents; red solid line: polynomial fit; black solid lines: 99% confidence intervals of the values of the fitted curve.

According to the prescription of Sec. VE the one which minimizes the dispersion of the data around the fitted curve is the first one, i.e.,  $\tau_{\max} = 2798$ . In Figs. 5 and 6 we report all the relevant steps for the computation of  $H(0.1)$  and  $H(1)$  as described in Sec. VB with the figures arranged as in Fig. 3.

The empirical scaling appears to settle in both cases on the asymptotic straight line found by the algorithm (see Figs. 5 and 6), and the values of  $\tau_{\min}$  found are

$$\hat{\tau}_{\min}^{H(0.1)} = 255, \quad \hat{\tau}_{\min}^{H(1)} = 815. \quad (38)$$

Again subfigures (e) and (f), in both cases, prove that, for this empirical dataset as well, for high values of  $x = \ln \tau$  the filter function  $g(x)$  oscillates around zero and that its integral converges. We notice also that in Fig. 6 the choice of the local maximum may seem puzzling, since other apparently better candidates appear on its right. However, we recall that the local maximum is chosen in order to achieve the best parabolic fit of the integrated scaling in the adjusted coefficient of determination sense. In order to complete our analysis of the scaling properties of the AXP time series we report in Fig. 7

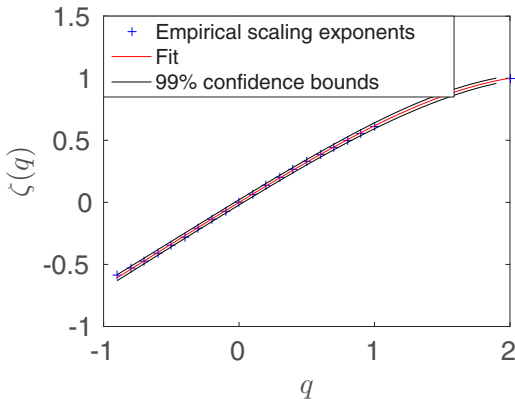


FIG. 15. Fitted empirical scaling exponents for MAR time series. Blue crosses: empirical scaling exponents; red solid line: polynomial fit; black solid lines: 99% confidence intervals of the values of the fitted curve.

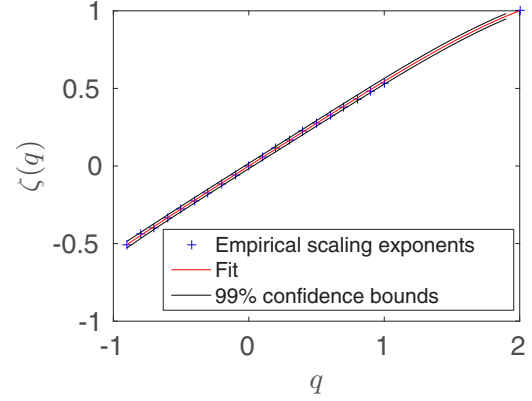


FIG. 16. Fitted empirical scaling exponents for MMM time series. Blue crosses: empirical scaling exponents; red solid line: polynomial fit; black solid lines: 99% confidence intervals of the values of the fitted curve.

the fit of all the scaling exponents we measured. In this case we found a second degree polynomial fit to be appropriate with the coefficients equal to

$$\hat{B} = -0.052 \quad (-0.058, -0.045), \quad (39)$$

where we reported in parentheses the 95% confidence interval of the estimated coefficients.

### C. Other data

In this section we report the application of the method to the following empirical time series: Abbott Laboratories (ABT), AECOM (ACM), Adobe Systems (ADBE), American International Group (AIG), Advanced Micro Devices Inc. (AMD), Google (GOOGL), Honeywell International Inc. (HON), Marriott International (MAR), 3M Company (MMM), and Procter & Gamble (PG). All time series are taken between 12 October 2015 and 11 November 2015 on a tick-by-tick basis and traded on the NYSE. Details concerning the length of each time series, the values of  $\tau_{\max}$  and the application of

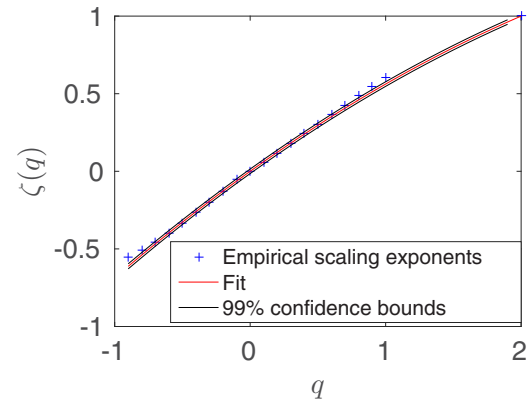


FIG. 17. Fitted empirical scaling exponents for PG time series. Blue crosses: empirical scaling exponents; red solid line: polynomial fit; black solid lines: 99% confidence intervals of the values of the fitted curve.

the method are reported in Table II, along with the results of AXP discussed in the previous subsection. If we found a parabolic fit appropriate, the value of  $\hat{B}$  is given, otherwise if we found a quartic fit appropriate, the values of  $\hat{D}$  and  $\hat{C}$  are given (see Sec. VE) in both cases along with the 95% interval. In Figs. 8–17 we report instead for each empirical time series the measured scaling exponents in blue crosses, the fitted polynomial in red solid line and the 99% confidence interval of the fitted functions in black solid lines. From Table II it appears that there is no clear preference for the parabolic or the quartic polynomial fit, which is in turn linked to the complexity of the underlying generating process. For four time series out of six for which the fourth degree polynomial is more suitable, we notice that the value of  $\hat{C}$  can be assumed to be zero, which reflects in a symmetric singularity spectrum (cf. Sec. II).

### VIII. CONCLUSIONS

We proposed a method to measure the scaling exponents of financial time series, discussing how the discreteness of the available data sets, for both synthetic and real time series, affects the scaling measures. In particular we showed that the exact power law scaling of the moments holds for multi- and unscaling processes continuous in time, while it does not for their discrete counterparts, and it appears to be recovered only in the high aggregation limit. We argued then that the scaling of discrete processes, which corresponds to a multi- or unscaling process continuous in time, whether synthetic or real, should be corrected via a filter function. According to our interpretation of the results, the need of this filter function arises when a process is not stable under aggregation, which means that, for discrete processes, the distribution of the increments at the finest scale is different with respect to the one at gross scale, i.e., in the continuous time limit. In order to circumvent this problem we devised a numerical method to subtract the filter function from the underlying linear scaling, without the need of knowing its exact functional form. Finally we smoothed the measured scaling exponents by fitting them with either a second or a fourth degree polynomial, which, taking into account the theoretical requirement of the multifractal picture, reduce to have respectively one and two degrees of freedom. In general terms, a higher degree corresponds to a higher degree of complexity of the underlying generating process.

We found that there are few qualitative features common to all stocks concerning the behavior of the filter function. For positive moments, almost always the scaling clearly converges to the asymptotic behavior found by our algorithm from above. However, a different behavior of the overall shape of the convergence is found for values of  $q$  near zero and values of  $q$  near one, with a transient between the two regimes. In particular for values of  $q$  near zero the empirical scaling crosses its asymptotic inferred behavior from below finally settling on it from above, while, for all but one time series (ABT), for  $q$  near one the empirical scaling stays always above the asymptotic one before settling on it again from above. From another perspective it means that positive absolute moments near the first one tend to be always overestimated, whatever the aggregation, while small absolute moments tend to be underestimated for small aggregations while overestimated otherwise. As for the negative absolute moments the convergence

pattern is stockwise: in some cases the scaling lies always above the asymptotic scaling converging from above, in others it starts above, then it crosses the asymptotic scaling and finally converges from below. We report that this change of behavior dependent on the order of the measured moment is absent for the MRW, where the convergence, for positive absolute moments, happens from above, while for negative ones it happens from below. We argue that this difference may arise from the fact that the innovations of a MRW, also at its finest scale, are (conditionally Gaussian) random variables continuous in value, whereas real financial tick-by-tick data are intrinsically discrete, due to the presence of a minimum tick size (cf., for example, Ref. [57]). It is worth noting that this feature of tick-by-tick data does not affect the coherence of our work since the goal of our method is to measure the scaling behavior in a high aggregation regime, where returns can be considered continuous in value. We stress that this convergence has been found in the so-called trading time, which is inhomogeneous. Different approaches have been developed to deal with time inhomogeneity of tick-by-tick data (see, for example, Refs. [2,63,64]); however, we decided to avoid to introduce such techniques both because we performed a univariate analysis and because we preferred to avoid to introduce a source of arbitrariness coming from the choice of a specific procedure. Finally we report that as for the overall shape of the function  $\zeta(q)$ , we found that in our data set there is no clear preference between the second or the fourth degree considered polynomials, despite in four cases out of six, where the fourth degree polynomial fit was found more suitable, the coefficient of the third degree term can be assumed to be zero within the error bounds.

For future developments we are planning to study the consequences of these considerations on the scaling in the physical time, which, making the time series synchronous, would give us a natural setting in order to extend our approach to the study of the multivariate multifractality [65,66].

### ACKNOWLEDGMENTS

The authors wish to thank Bloomberg for providing the data. T.D.M. wishes to thank the COST Action TD1210 for partially supporting this work. T.A. acknowledges support of the UK Economic and Social Research Council (ESRC) in funding the Systemic Risk Centre (ES/K002309/1).

### APPENDIX A: EXPLICIT COMPUTATION OF EQ. (20)

In order to understand the scaling properties of the moments of  $S_N$  in the continuous time limit we need first to know its pdf  $S_N$ , namely,  $p_s(S_N)$ . From the probability theory we know that this pdf is given by the convolution of the single pdfs, for example,

$$\begin{aligned} p_s(S_2) &= p(x_1) * p(x_2) = \int_{\mathbb{R}} dx_1 p(x_1) p(S_2 - x_1), \\ p_s(S_3) &= p(x_1) * p(x_2) * p(x_3) \\ &= \int_{\mathbb{R}} dS_2 \int_{\mathbb{R}} dx_1 p(x_1) p(S_2 - x_1) p(S_3 - S_2). \end{aligned} \quad (\text{A1})$$

In general, defining  $S_0 = 0$ ,

$$p_s(S_N) = \prod_{i=1}^{N-1} \int_{\mathbb{R}} dS_i p(S_i - S_{i-1}) p(S_N - S_{N-1}). \quad (\text{A2})$$

If we consider the discrete case what we usually compute after shuffling is

$$\begin{aligned} E[|S_N|^q] &= \int_{\mathbb{R}} dS_N |S_N|^q p_s(S_N) \\ &= \int_{\mathbb{R}} dS_N |S_N|^q \prod_{i=1}^{N-1} \\ &\quad \times \int_{\mathbb{R}} dS_i p(S_i - S_{i-1}) p(S_N - S_{N-1}). \end{aligned} \quad (\text{A3})$$

It is evident that the dependence of  $E[|S_N|^q]$  from the time horizon  $\tau = N\Delta t$  is certainly far from being a simple power law as requested by the multifractal picture [see Eq. (4)]. Thus, this is why the numerical estimations are horizon-dependent. However, analytically, in order to infer something about the multi- or unscaling nature of the process  $x_i$ , we are interested in the continuous time limit of Eq. (A3), in line with the underlying assumptions of multifractality. In particular we want to compute the simultaneous limits  $\Delta t \rightarrow 0$ ,  $N \rightarrow \infty$ , but keeping the product  $N\Delta t = \tau$  fixed, in order to have finite time horizons. In formulas we want to compute

$$\lim_{\substack{\Delta t \rightarrow 0 \\ N \rightarrow \infty \\ N\Delta t = \tau}} E[|S_N|^q] = E[|S_\infty|^q] = \lim_{\substack{\Delta t \rightarrow 0 \\ N \rightarrow \infty \\ N\Delta t = \tau}} \int_{\mathbb{R}} dS_N |S_N|^q p_s(S_N). \quad (\text{A4})$$

Due to the CLT the following equality holds:

$$E[|S_\infty|^q] = \lim_{\substack{\Delta t \rightarrow 0 \\ N \rightarrow \infty \\ N\Delta t = \tau}} \int_{\mathbb{R}} dS_N |S_N|^q \frac{e^{-\frac{S_N^2}{2\sigma^2 N\Delta t}}}{\sqrt{2\pi\sigma\sqrt{N\Delta t}}}. \quad (\text{A5})$$

Using now the variable  $z = \frac{S_N}{\sqrt{\sigma^2 N\Delta t}}$ , Eq. (A5) becomes

$$E[|S_\infty|^q] = \lim_{\substack{\Delta t \rightarrow 0 \\ N \rightarrow \infty \\ N\Delta t = \tau}} \int_{\mathbb{R}} dz \sigma^q (N\Delta t)^{\frac{q}{2}} |z|^q \frac{e^{-\frac{z^2}{2}}}{\sqrt{2\pi}}. \quad (\text{A6})$$

Performing then the limit, taking out the constants and solving the integral (which is known), the solution is finally

$$E[|S_\infty|^q] = \sigma^q \frac{2^{\frac{q}{2}} \Gamma(\frac{q+1}{2})}{\sqrt{\pi}} \tau^{\frac{q}{2}}. \quad (\text{A7})$$

#### APPENDIX B: COMPUTATION OF THE VALUE OF $H(2)$ OF REAL FINANCIAL PROCESSES

In this Appendix we show that for empirical financial time series  $H(2) = 0.5$ . As noted in Ref. [42], on empirical financial

datasets the estimator of  $H(2)$  cannot be reliably measured because the second moment of the empirical distributions is finite, but the fourth momentum is often infinite (cf. Refs. [5,46]). Using empirical evidence, however, it is possible to infer its value in the limit of infinite aggregation. This simple result follows from the following properties of financial time series, calling  $r_\tau(t)$  the log returns:

$$\begin{aligned} E[r_\tau(t)] &= 0 \\ \text{Var}[r_\tau(t)] &< \infty \\ \text{Corr}[r_\tau(t_1), r_\tau(t_2)] &= 0 \quad t_1 \neq t_2, \end{aligned} \quad (\text{B1})$$

where Corr is the correlation function. We notice that in the high-frequency domain the third property is true after a few lags ([2,5]), thus it does not affect the asymptotic properties of the scaling. Let us call then  $\varepsilon_{\Delta t}(k)$  the elementary increments of a process satisfying the properties listed in Eq. (B1) with variance  $\text{Var}[\varepsilon_{\Delta t}(k)] = \sigma^2 \Delta t$ , where  $\sigma$  is a fixed scalar and  $\Delta t$  the discretization step. The returns of this process under aggregation can be written on scale  $\tau$  as

$$r_\tau(t) = \sum_{k=\frac{t}{\Delta t}+1}^{\frac{t+\tau}{\Delta t}} \varepsilon_{\Delta t}(k). \quad (\text{B2})$$

The following chain of equalities hold:

$$\begin{aligned} E[|r_\tau(t)|^2] &= \text{Var}[r_\tau(t)] = \text{Var}\left[\sum_{k=\frac{t}{\Delta t}+1}^{\frac{t+\tau}{\Delta t}} \varepsilon_{\Delta t}(k)\right] \\ &= \sum_{k=\frac{t}{\Delta t}+1}^{\frac{t+\tau}{\Delta t}} \text{Var}[\varepsilon_{\Delta t}(k)] \\ &\quad + \sum_{k_1 < k_2 = \frac{t}{\Delta t}+1}^{\frac{t+\tau}{\Delta t}} 2\text{Cov}[\varepsilon_{\Delta t}(k_1), \varepsilon_{\Delta t}(k_2)] \\ &= \sigma^2 \tau, \end{aligned} \quad (\text{B3})$$

where the first and fourth equalities follow from Eq. (B1). Thus, with the notation of Eq. (4), it can be written that

$$E[|r_\tau(t)|^2] = K(2)\tau^{2H(2)} = \sigma^2 \tau; \quad (\text{B4})$$

which in turn implies that  $H(2) = 0.5$ .

#### APPENDIX C: EFFECT OF THE CONCAVITY ON THE SCALING EXPONENTS FITTING FUNCTION

In this Appendix we derive the third condition in Eq. (32). The second derivative of Eq. (30) reads as

$$\zeta''(q) = 12Dq^2 + 6Cq + 2B. \quad (\text{C1})$$

To ensure that the condition  $\zeta''(q) < 0$  holds for every  $q$  the roots of (C1) must coincide and  $D < 0$ . In particular the roots of (C1) are

$$q_{\pm} = \frac{-3C \pm \sqrt{9C^2 - 24BD}}{12D}, \quad (\text{C2})$$

which, in order to coincide, must satisfy

$$B = \frac{3C^2}{8D}. \quad (\text{C3})$$

- [1] R. N. Mantegna and H. E. Stanley, *Introduction to Econophysics: Correlations and Complexity in Finance* (Cambridge University Press, Cambridge, 1999).
- [2] M. M. Dacorogna, R. Gençay, U. A. Müller, R. B. Olsen, and O. V. Pictet, *An Introduction to High-Frequency Finance* (Academic Press, San Diego, 2001).
- [3] R. N. Mantegna and H. E. Stanley, Scaling behavior in the dynamics of an economic index, *Nature (London)* **376**, 46 (1995).
- [4] T. Di Matteo, Multi-scaling in finance, *Quant. Finance* **7**, 21 (2007).
- [5] R. Cont, Empirical properties of asset returns: Stylized facts and statistical issues, *Quant. Finance* **1**, 223 (2001).
- [6] S. Ghoshghaie, W. Breymann, J. Peinke, P. Talkner, and Y. Dodge, Turbulent cascades in foreign exchange markets, *Nature (London)* **381**, 767 (1996).
- [7] L. E. Calvet and A. Fisher, Multifractality in asset returns: Theory and evidence, *Rev. Econ. Stat.* **84**, 381 (2002).
- [8] R. Liu, T. Di Matteo, and T. Lux, Multifractality and long-range dependence of asset returns: The scaling behavior of the Markov-switching multifractal model with lognormal volatility components, Kiel Working Papers 1427 (2008).
- [9] M. Bartolozzi, C. Mellen, T. Di Matteo, and T. Aste, Multi-scale correlations in different futures markets, *Eur. Phys. J. B* **58**, 207 (2007).
- [10] M. Bartolozzi, C. Mellen, F. Chan, D. Oliver, T. Di Matteo, and T. Aste, Applications of physical methods in high-frequency futures markets, *Proc. SPIE* **6802**, 680203 (2007).
- [11] L. Kristoukek, Fractal markets hypothesis and the global financial crisis: Scaling, investment horizons and liquidity, *Adv. Complex Syst.* **15**, 1250065 (2012).
- [12] Z.-Q. Jiang and W.-X. Zhou, Multifractality in stock indexes: Fact or fiction? *Physica A* **387**, 3605 (2008).
- [13] T. Lux, Detecting multi-fractal properties in asset returns: The failure of the scaling estimator, *Int. J. Mod. Phys. C* **15**, 481 (2004).
- [14] D. Grech and Z. Mazur, On the scaling ranges of detrended fluctuation analysis for long-term memory correlated short series of data, *Physica A* **392**, 2384 (2013).
- [15] D. Grech and Z. Mazur, Scaling range of power laws that originate from fluctuation analysis, *Phys. Rev. E* **87**, 052809 (2013).
- [16] L. G. Moyano, J. De Souza, and S. M. Duarte Queirós, Multifractal structure of traded volume in financial markets, *Physica A* **371**, 118 (2006).
- [17] J. de Souza and S. M. Duarte Queirós, Effective multifractal features of high-frequency price fluctuations time series and  $\ell$ -variability diagrams, *Chaos Solitons Fractals* **42**, 2512 (2009).
- [18] R. Morales, T. Di Matteo, R. Gramatica, and T. Aste, Dynamical generalized hurst exponent as a tool to monitor unstable periods in financial time series, *Physica A* **391**, 3180 (2012).
- [19] W.-X. Zhou, Multifractal detrended cross-correlation analysis for two nonstationary signals, *Phys. Rev. E* **77**, 066211 (2008).
- [20] G.-F. Gu and W.-X. Zhou, Detrending moving average algorithm for multifractals, *Phys. Rev. E* **82**, 011136 (2010).
- [21] W.-X. Zhou, Finite-size effect and the components of multifractality in financial volatility, *Chaos Solitons Fractals* **45**, 147 (2012).
- [22] N. Nava, T. Di Matteo, and T. Aste, Time-dependent scaling patterns in high frequency financial data, *Eur. Phys. J. Spec. Top.* **225**, 1997 (2016).
- [23] N. Nava, T. Di Matteo, and T. Aste, Anomalous volatility scaling in high frequency financial data, *Physica A* **447**, 434 (2016).
- [24] L. E. Calvet, A. J. Fisher, and B. B. Mandelbrot, A multifractal model of asset returns, Cowles Foundation Discussion Paper No. 1164 (1997).
- [25] L. E. Calvet and A. Fisher, Forecasting multifractal volatility, *J. Econometrics* **105**, 27 (2001).
- [26] T. Lux, The markov-switching multifractal model of asset returns: GMM estimation and linear forecasting of volatility, *J. Bus. Econ. Stat.* **26**, 194 (2008).
- [27] T. Lux and L. Morales-Arias, Forecasting volatility under fractality, regime-switching, long memory and student innovations, *Comput. Stat. Data Anal.* **54**, 2676 (2010).
- [28] M. Segnon and T. Lux, *Multifractal models in finance: Their origin, properties, and applications*, Kiel Working Paper (2013).
- [29] R. Liu, T. Di Matteo, and T. Lux, True and apparent scaling: The proximity of the Markov-switching multifractal model to long-range dependence, *Physica A* **383**, 35 (2007).
- [30] E. Bacry, J. Delour, and J.-F. Muzy, Multifractal random walk, *Phys. Rev. E* **64**, 026103 (2001).
- [31] J.-F. Muzy and E. Bacry, Multifractal stationary random measures and multifractal random walks with log infinitely divisible scaling laws, *Phys. Rev. E* **66**, 056121 (2002).
- [32] E. Bacry and J.-F. Muzy, Log-infinitely divisible multifractal processes, *Commun. Math. Phys.* **236**, 449 (2003).
- [33] E. Bacry, L. Duvernet, and J.-F. Muzy, Continuous-time skewed multifractal processes as a model for financial returns, *J. Appl. Probab.* **49**, 482 (2012).
- [34] L. E. Calvet and A. J. Fisher, How to forecast long-run volatility: Regime switching and the estimation of multifractal processes, *J. Financial Econometrics* **2**, 49 (2004).
- [35] E. Bacry, A. Kozhemyak, and J.-F. Muzy, Continuous cascade models for asset returns, *J. Econ. Dyn. Control* **32**, 156 (2008).
- [36] E. Bacry, A. Kozhemyak, and J. F. Muzy, Log-normal continuous cascade model of asset returns: Aggregation properties and estimation, *Quant. Finance* **13**, 795 (2013).
- [37] J. W. Kantelhardt, S. A. Zschiegner, E. Koscielny-Bunde, S. Havlin, A. Bunde, and H. E. Stanley, Multifractal detrended fluctuation analysis of nonstationary time series, *Physica A* **316**, 87 (2002).
- [38] T. Di Matteo, T. Aste, and M. M. Dacorogna, Scaling behaviors in differently developed markets, *Physica A* **324**, 183 (2003).
- [39] T. Di Matteo, T. Aste, and M. M. Dacorogna, Long-term memories of developed and emerging markets: Using the scaling analysis to characterize their stage of development, *J. Bank. Finance* **29**, 827 (2005).
- [40] J. Barunik and L. Kristoufek, On hurst exponent estimation under heavy-tailed distributions, *Physica A* **389**, 3844 (2010).
- [41] A. Arneodo, E. Bacry, and J. F. Muzy, The thermodynamics of fractals revisited with wavelets, *Physica A* **213**, 232 (1995).
- [42] R. J. Buonocone, T. Aste, and T. Di Matteo, Measuring multiscaling in financial time-series, *Chaos Solitons Fractals* **88**, 38 (2016).
- [43] W.-X. Zhou, The components of empirical multifractality in financial returns, *Europhys. Lett.* **88**, 28004 (2009).

- [44] J. Barunik, T. Aste, T. Di Matteo, and R. Liu, Understanding the source of multifractality in financial markets, *Physica A* **391**, 4234 (2012).
- [45] E. Green, W. Hanan, and D. Heffernan, The origins of multifractality in financial time series and the effect of extreme events, *Eur. Phys. J. B* **87**, 1 (2014).
- [46] A. Chakraborti, I. M. Toke, M. Patriarca, and F. Abergel, Econophysics review: I. Empirical facts, *Quant. Finance* **11**, 991 (2011).
- [47] L. E. Calvet, A. Fisher, and B. Mandelbrot, Large deviations and the distribution of price changes, Cowles Foundation Discussion Paper No. 1165 (1997).
- [48] T. C. Halsey, M. H. Jensen, L. P. Kadanoff, I. Procaccia, and B. I. Shraiman, Fractal measures and their singularities: The characterization of strange sets, *Phys. Rev. A* **33**, 1141 (1986).
- [49] R. Benzi, G. Paladin, G. Parisi, and A. Vulpiani, On the multifractal nature of fully developed turbulence and chaotic systems, *J. Phys. A* **17**, 3521 (1984).
- [50] L. E. Calvet, A. J. Fisher, and B. B. Mandelbrot, Multifractality of Deutschmark/US dollar exchange rates, Cowles Foundation Discussion Paper No. 1166 (1997).
- [51] A.-L. Barabási and T. Vicsek, Multifractality of self-affine fractals, *Phys. Rev. A* **44**, 2730 (1991).
- [52] N. L. Johnson, S. Kotz, and N. Balakrishnan, *Continuous Univariate Distributions, Wiley Series in Probability and Mathematical Statistics: Applied Probability and Statistics*, Vol. 2 (John Wiley & Sons, New York, 1995).
- [53] H. Nakao, Multi-scaling properties of truncated Lévy flights, *Phys. Lett. A* **266**, 282 (2000).
- [54] A. V. Chechkin and V. Yu Gonchar, Self and spurious multi-affinity of ordinary Levy motion, and pseudo-Gaussian relations, *Chaos Solitons Fractals* **11**, 2379 (2000).
- [55] K. Abadir and J. Magnus, The central limit theorem for Student's distribution—Solution, *Econometric Theory* **20**, 1261 (2004).
- [56] E. Bacry, J. Delour, and J. F. Muzy, Modelling financial time series using multifractal random walks, *Physica A* **299**, 84 (2001).
- [57] J.-P. Bouchaud, M. Mézard, and M. Potters, Statistical properties of stock order books: Empirical results and models, *Quant. Finance* **2**, 251 (2002).
- [58] M. S. Bartlett, On the theoretical specification and sampling properties of autocorrelated time-series, *Supplement to J. R. Stat. Soc.* **8**, 27 (1946).
- [59] Z. Ding, C. W. J. Granger, and R. F. Engle, A long memory property of stock market returns and a new model, *J. Empirical Finance* **1**, 83 (1993).
- [60] H. Theil, *Economic Forecasts and Policy*, 2nd ed. (North-Holland, Amsterdam, 1961).
- [61] P. Bloomfield and W. Steiger, Least absolute deviations curve-fitting, *SIAM J. Sci. Stat. Comput.* **1**, 290 (1980).
- [62] B. B. Mandelbrot, P. H. Cootner, R. E. Gomory, E. F. Fama, W. S. Morris, and H. M. Taylor, *Fractals and Scaling in Finance: Discontinuity, Concentration, Risk, Selecta Volume E*. (Springer, New York, 2013).
- [63] J. R. Russel and R. F. Engle, Analysis of high frequency financial data, in *Handbook of Financial Econometrics, Vol 1: Tools and Techniques*, Handbooks in Finance, edited by A.-S. Yacine and H. L. Peter (Elsevier Science, San Diego, 2009), Chap. 7, pp. 383–426.
- [64] A. Dupuis and R. B. Olsen, High frequency finance: Using scaling laws to build trading models, in *Handbook of Exchange Rates* (John Wiley & Sons, Inc., New York, 2012), pp. 563–584.
- [65] C. Meneveau, K. R. Sreenivasan, P. Kailasnath, and M. S. Fan, Joint multifractal measures: Theory and applications to turbulence, *Phys. Rev. A* **41**, 894 (1990).
- [66] W.-J. Xie, Z.-Q. Jiang, G.-F. Gu, X. Xiong, and W.-X. Zhou, Joint multifractal analysis based on the partition function approach: Analytical analysis, numerical simulation and empirical application, *New J. Phys.* **17**, 103020 (2015).